

Unconventional superconducting gap via spin fluctuations in iron-vacancy ordered $A_y\text{Fe}_{2-x}\text{Se}_2$

Shin-Ming Huang¹ and Chung-Yu Mou^{1,2,3}

¹*Department of Physics, National Tsing Hua University, Hsinchu 30043, Taiwan*

²*Institute of Physics, Academia Sinica, Nankang, Taiwan and*

³*Physics Division, National Center for Theoretical Sciences, P.O.Box 2-131, Hsinchu, Taiwan*

Based on an effective 12-orbital tight-binding model, we examine the superconducting states induced by the antiferromagnetic fluctuations for iron-vacancy-ordered $A_y\text{Fe}_{2-x}\text{Se}_2$. It is shown that due to the broken reflection symmetry of the iron vacancies, new superconducting states with C_{4h} symmetry emerges. In particular, we show that the in the C_{4h} symmetry, zeros of angles for the pairing momenta are free parameters. Hence there are more degrees of freedoms to characterize the superconducting gaps, which can further increase the gain of the condensation energy. Nonetheless, similar to other iron-based superconductors, the singlet ground state is still dominated by s -wave or d -wave, which are nearly degenerate with anisotropic gaps. Furthermore, s -wave and d -wave superconducting states are separated by a quantum critical point controlled by the Hund's rule coupling J_H .

PACS numbers: 74.70.Xa, 74.20.Mn, 74.20.Rp

I. INTRODUCTION

Since the discovery of high-temperature superconductivity in cuprates, it has been a key interest to find the mechanism that causes the high T_c and its unconventional. After more than 20 years of intensive investigations, however, the origin of high- T_c superconductivity in cuprates is still not understood. The discovery of relatively high T_c in iron-based superconductors^{1,2} appears to opens a different route for high-temperature superconductivity and thus provides a unique opportunity to reclarify the physics of the unconventional superconductivity. One of the features for the unconventional superconductivity is appearance of the sign-switched gap function. The presence of disconnected Fermi surface (FS) sheets in iron-based superconductors is an ingenious condition for the sign-switched order parameters, both for s_{\pm} -wave and d -wave³. It is widely believed that the superconducting (SC) pairing is driven by the crucial inter-FS-sheet scattering or equivalently by the antiferromagnetic (AFM) fluctuations⁴⁻⁶ since the former process also leads to a strong AFM correlation.

The recent discovery of alkaline-intercalated iron-selenide superconductor $A_y\text{Fe}_{2-x}\text{Se}_2$ with T_c above 30K⁷ initiates an interesting branch for exploring the superconductivity in iron-based superconductors. The chemically-stable structure $A_{0.8}\text{Fe}_{1.6}\text{Se}_2$ exhibits a $\sqrt{5} \times \sqrt{5}$ iron-vacancy order and the block-checkerboard antiferromagnetism⁸⁻¹⁰. By varying iron or alkaline content, the AFM state becomes unstable and the SC state appears^{11,12}. Lately, many experiments indicate that antiferromagnetism and superconductivity are phase separated¹³⁻¹⁸; especially in a recent scanning tunneling microscopy (STM) measurement¹⁹, it is shown that the sample is separated into two difference phases, SC KFe_2Se_2 and insulating $\text{K}_x\text{Fe}_{1.6}\text{Se}_2$. Nevertheless, it needs further study if the insulating region can be altered

into a metal by chemical doping or by applying pressure. First-principles simulation of the pressure effects shows that by applying pressure with the $\sqrt{5} \times \sqrt{5}$ iron-vacancy order, the system undergoes two successive magnetic transitions, from the semiconducting block-checkerboard AFM phase to the metallic stripe (collinear) AFM phase and then to a metallic non-magnetic phase²⁰. These results agree with transport measurements that the pressure induces a semiconductor-to-metal transition²¹; however, it remains confusing that experimentally as the system became more metallic with pressure, T_c got smaller. Whether it suggests the necessity of strong correlation for superconductivity would be an interesting question.

Nuclear magnetic resonance (NMR) experiments find singlet superconductivity and no pronounced spin fluctuations near T_c ²³⁻²⁵. The spin-lattice relaxation rate $1/T_1T$ shows no Hebel-Slichter coherence peak and a power-law behavior below T_c , indicating an unconventional SC gap (very likely gapless). Although salient spin fluctuations are not present in NMR, the possibility of spin-fluctuation-driven superconductivity should not be excluded since the information of spin fluctuations would be hidden in signals²⁶. Raman measurement within the two-magnon scattering window shows that the signal grows up approaching T_c and undergoes a sudden drop when entering the SC phase²⁷, supporting that superconductivity arises from magnetic fluctuations.

Theoretically, previous works²⁸⁻³² on superconductivity in $A_y\text{Fe}_{2-x}\text{Se}_2$ were based on the band structure of KFe_2Se_2 ^{33,34}. However, the iron-vacancy order has been proved to make a big change in the FS shape^{10,35}, though not confirmed so far by angle-resolved photoemission spectroscopy (ARPES)³⁶⁻³⁹. Therefore, if superconductivity could happen in the iron-vacancy ordering phase, it is crucial to examine the pairing symmetry and pairing mechanism.

In this work, we investigate superconducting instability in iron-vacancy-ordered $A_y\text{Fe}_{2-x}\text{Se}_2$. Previously,

based on the 12-orbital tight-binding model that fits the band structure of $\text{K}_y\text{Fe}_{2-x}\text{Se}_2$, we have studied the magnetic phase in the generalized Hubbard model and succeeded in explaining the block-checkerboard AFM instability from the Stoner's theory⁴⁰. Here based on the same tight-binding model and starting from a non-magnetic metallic phase, we examine the superconductivity by the fluctuation-exchange (FLEX) approach^{41,42}. For singlet superconductivity, we examine the pairing coupling constants for s -wave and d -wave states from the effective scattering matrix and find that s -wave and d -wave are closely degenerate as what happen in other iron-pnictide superconductors⁶. The gap functions in both symmetries are highly anisotropic and have nodes. Furthermore, since the iron-vacancy order lowers the symmetry of $\text{A}_y\text{Fe}_{2-x}\text{Se}_2$ to the group C_{4h} , the gap functions do not need to be reflection symmetric and this implies that there are degrees of freedom in defining zeros of angles for the pairing momenta. These extra degrees of freedom for the gap function can further increase the gain of the condensation energy. The symmetry of the system is controllable by tuning the Hund's rule coupling J_H and the critical value at about $J_H = 0.2U$. The Hund's rule coupling manipulates the phase transition or crossover in superconductivity, antiferromagnetism⁴⁰, or even the metallic transport⁴³, emphasizing the substantial rules of orbital-correlation in the multi-orbital electronic system.

II. THEORETICAL METHOD

The vacancy ordered iron selenide $\text{A}_y\text{Fe}_{2-x}\text{Se}_2$ is a system with one-fifth of Fe being taken off and forming a characteristic $\sqrt{5} \times \sqrt{5}$ pattern (Fig. 1(a)). The presence of the iron vacancy changes the space group from $I4/mmm$ (D_{4h}) to $I4/m$ (C_{4h}). As a result, the four-fold rotational symmetry is retained without the reflection symmetry with respect to the xz , yz and the diagonal planes. The absence of reflection symmetry implies that there is no symmetry axis. Hence there is an extra degree of freedom in defining the zero value of angles for basis functions of C_{4h} . For instance, the basis function $\cos(4\theta)$ becomes $\cos[4(\theta - \theta_0)]$ with θ_0 being a free parameter.

To implement the $I4/m$ symmetry for $\text{A}_y\text{Fe}_{2-x}\text{Se}_2$, we have constructed a 12-orbital tight-binding model with four Fe atoms per cell and three t_{2g} orbitals per Fe to investigate the magnetic instability⁴⁰. The resulting FS is shown in Fig. 1(b) with two hole pockets, α_1 the one centering on $(0,0)$ and α_2 on (π,π) , and four electron pockets, β_1 the one and its inversion around $\pm(\pi/2, \pi/2)$ and β_2 around $\pm(-\pi/2, \pi/2)$. To calculate the SC gap, we shall divide the k space into 200×200 lattice point and approximate states on the FS sheets by picking totally 216 k points with 44 points on FS- α_1 , 40 points on FS- α_2 , and 66 points both on FS- β_1 and β_2 . These k points on FS sheets are characterized by angles, $\theta_{\alpha 1}$, $\theta_{\alpha 2}$, $\theta_{\beta 1}$, and $\theta_{\beta 2}$ as illustrated in Fig. 1(b). All angles are relative to the horizontal k_x axis except that $\theta_{\beta 2}$ is relative to the

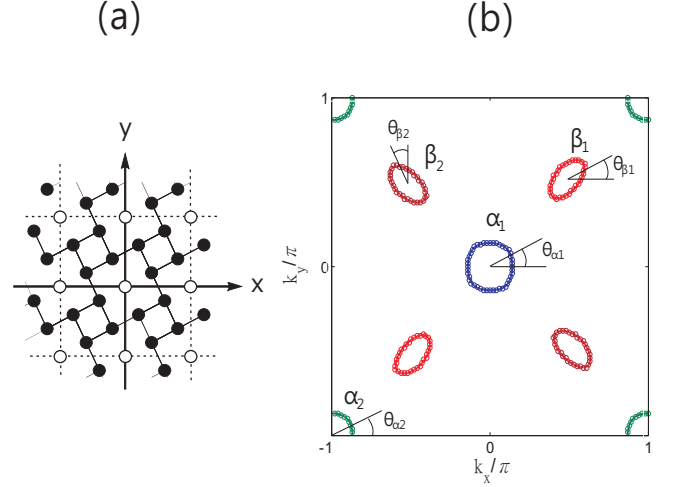


FIG. 1: (Color online) (a) The illustration of the Fe plane with the left-chiral $\sqrt{5} \times \sqrt{5}$ vacancy ordering. The solid circles denote Fe atoms and the empty ones the vacancies. Every four nearest vacancies enclose the unit cells. x and y are the primitive vectors. (b) The Fermi surface results from the 12-orbital tight-binding model: two hole pockets (α_1 and α_2) and four electron pockets (β_1 and β_2 and their inverse partners). 216 k -points on the Fermi surfaces are selected and shown by circles (zoom in to see). Points on FS- α_1 , α_2 , β_1 and β_2 are parameterized by the angles, $\theta_{\alpha 1}$, $\theta_{\alpha 2}$, $\theta_{\beta 1}$, and $\theta_{\beta 2}$, respectively.

vertical k_y axis due to that the FS- β_2 is a 90° rotation from FS- β_1 .

We shall assume that the interaction between electrons on each Fe atom is given by the generalized Hubbard model,

$$H_I = \sum_i \sum_{I=1}^4 \left\{ U \sum_{a=1}^3 n_{aI, i\uparrow} n_{aI, i\downarrow} + \sum_{a,b(a>b)} \left[\left(U' - \frac{J_H}{2} \right) n_{aI, i} n_{bI, i} - 2J_H \mathbf{S}_{aI, i} \cdot \mathbf{S}_{bI, i} + J_C \left(d_{aI, i\uparrow}^\dagger d_{aI, i\downarrow}^\dagger d_{bI, i\downarrow} d_{bI, i\uparrow} + h.c. \right) \right] \right\}, \quad (1)$$

where I is for four Fe atoms and a is for three t_{2g} orbitals. It was found⁴⁰ that as the interaction turns on, the spin fluctuation is strong at $\mathbf{q} = (\pi, \pi)$ and $(\pi, 0)$, in which the former is related to the checkerboard antiferromagnetism and the latter is related to the stripe antiferromagnetism. These two magnetic states competes each other and the preference between them is controlled by the Hund's rule coupling, J_H .

The strong spin fluctuation is a possible pairing mechanism. To investigate the superconductivity arising from the exchange of spin and charge fluctuations, we follow the FLEX approach^{41,42}, in which the effective singlet

pairing scattering matrix is given by

$$\Gamma_{cd}^{ab}(\mathbf{k}, \mathbf{k}'; \omega) = \left[\frac{3}{2} \Gamma_s \chi_{RPA}^s(\mathbf{k} - \mathbf{k}', \omega) \Gamma_s + \frac{1}{2} \Gamma_s \right. \\ \left. - \frac{1}{2} \Gamma_c \chi_{RPA}^c(\mathbf{k} - \mathbf{k}', \omega) \Gamma_c + \frac{1}{2} \Gamma_c \right]_{cd}^{ab}, \quad (2)$$

where a, b, c , and d as before are orbital indices. In Eq. (2), the spin and charge vertices Γ_s and Γ_c are $\Gamma_s^{\tau\tau, \tau\tau} = U$, $\Gamma_s^{\tau\tau', \tau\tau'} = U'$, $\Gamma_s^{\tau\tau, \tau'\tau'} = J_H$, $\Gamma_s^{\tau\tau', \tau'\tau} = J_C$, and $\Gamma_c^{\tau\tau, \tau\tau} = U$, $\Gamma_c^{\tau\tau', \tau\tau'} = -U' + 2J_H$, $\Gamma_c^{\tau\tau, \tau'\tau'} = 2U' - J_H$, $\Gamma_c^{\tau\tau', \tau'\tau} = J_C$, where non-vanishing vertices are only between the same Fe, and τ denotes orbitals and $\tau \neq \tau'$. In the following, we will take the relations $U' = U - 2J_H$ and $J_C = J_H$. The random phase approximation (RPA) spin and charge susceptibilities are given by

$$\chi_{RPA}^s(\mathbf{q}, \omega) = \chi_0(\mathbf{q}, \omega) [1 - \Gamma_s \chi_0(\mathbf{q}, \omega)]^{-1}, \quad (3)$$

$$\chi_{RPA}^c(\mathbf{q}, \omega) = \chi_0(\mathbf{q}, \omega) [1 + \Gamma_c \chi_0(\mathbf{q}, \omega)]^{-1}, \quad (4)$$

with the bare susceptibility being given as

$$[\chi_0(\mathbf{q}, \omega)]_{ab}^{cd} = -\frac{1}{N} \sum_{\mathbf{k}, \mu, \nu} A_{c\mu}(\mathbf{k}) A_{a\mu}^*(\mathbf{k}) A_{b\nu}(\mathbf{k} + \mathbf{q}) A_{d\nu}^*(\mathbf{k} + \mathbf{q}) \\ \times \frac{n_F[E_\mu(\mathbf{k})] - n_F[E_\nu(\mathbf{k} + \mathbf{q})]}{\omega + E_\mu(\mathbf{k}) - E_\nu(\mathbf{k} + \mathbf{q}) + i\delta}, \quad (5)$$

where $A_{a\mu}$ is the orbital-band transformation matrix, $\psi_a(\mathbf{k}) = \sum_{\mu} A_{a\mu}(\mathbf{k}) \gamma_{\mu}(\mathbf{k})$. Here $\chi_0(\mathbf{q}, \omega)$ is calculated by using the bare Green's function not the dressed one. The low energy physics of the scattering matrix is projected to scattering among the FS sheets. We shall denote the scattering matrix with a Cooper pair from $(\mathbf{k}', -\mathbf{k}')$ on FS- ν scattered to $(\mathbf{k}, -\mathbf{k})$ on FS- μ by $\tilde{\Gamma}_{\mu\nu}(\mathbf{k}, \mathbf{k}')$,

$$\tilde{\Gamma}_{\mu\nu}(\mathbf{k}, \mathbf{k}') = \text{Re} \left\{ \sum_{a,b,c,d} A_{a\mu}^*(\mathbf{k}) A_{d\mu}^*(-\mathbf{k}) \right. \\ \left. \times \Gamma_{cd}^{ab}(\mathbf{k}, \mathbf{k}') A_{b\nu}(\mathbf{k}') A_{c\nu}(-\mathbf{k}') \right\}. \quad (6)$$

Since we consider even parity pairing, we evenly symmetrize the scattering matrix as $\tilde{\Gamma}_{\mu\nu}^{even}(\mathbf{k}, \mathbf{k}') = \frac{1}{2} [\tilde{\Gamma}_{\mu\nu}(\mathbf{k}, \mathbf{k}') + \tilde{\Gamma}_{\mu\nu}(\mathbf{k}, -\mathbf{k}')]$.

For a given gap function $g(\mathbf{k})$, a dimensionless coupling constant is defined by⁴⁴

$$\lambda = \frac{-\frac{1}{N_p} \sum_{\mu, \nu} \sum_{\mathbf{k}, \mathbf{k}'} \frac{1}{v_F(\mathbf{k}) v_F(\mathbf{k}')} g(\mathbf{k}) \tilde{\Gamma}_{\mu\nu}^{even}(\mathbf{k}, \mathbf{k}') g(\mathbf{k}')}{\sum_{\mu} \sum_{\mathbf{k}} \frac{1}{v_F(\mathbf{k})} g^2(\mathbf{k})}. \quad (7)$$

Here \mathbf{k} and \mathbf{k}' are restricted within FS μ and ν , respectively. $v_F(\mathbf{k}) = |\nabla_{\mathbf{k}} E_{\mu}(\mathbf{k})|$ is the Fermi velocity, and N_p ($=216$) is the number of \mathbf{k} on Fermi surfaces we choose. The coupling constant includes contributions from pocket-pocket scattering processes, and it is helpful

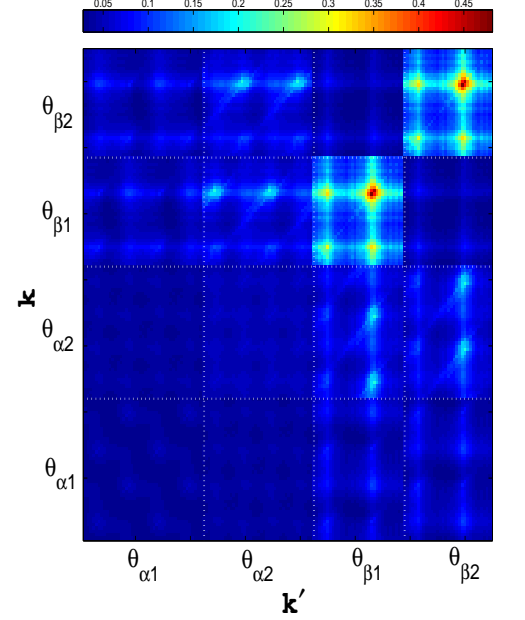


FIG. 2: (Color online) The weighted scattering matrix $[v_F(\mathbf{k})v_F(\mathbf{k}')]^{-1} \tilde{\Gamma}_{\mu\nu}^{even}(\mathbf{k}, \mathbf{k}')$ for \mathbf{k}, \mathbf{k}' being parametrized by $\theta_{\alpha 1}$, $\theta_{\alpha 2}$, $\theta_{\beta 1}$, and $\theta_{\beta 2}$ as defined in Fig. 1. θ 's turn around their corresponding Fermi surfaces from 0° to 360° . The dotted white lines separates different FS sheets. Here $U=1.0eV$ and $J_H=0.2U$ are used.

to extract them and to denote by a matrix $(\hat{\lambda})_{\mu\nu}$, satisfying $\lambda = \sum_{\mu, \nu} (\hat{\lambda})_{\mu\nu}$, where μ, ν refer to FS sheets, $\mu, \nu=1$ to α_1 , 2 to α_2 , 3 to β_1 , and 4 to β_4 .

The stationary condition in Eq. (7) ($\delta \lambda [g(\mathbf{k})] / \delta g(\mathbf{k}) = 0$) leads to the eigenvalue problem

$$-\frac{1}{N_p} \sum_{\mathbf{k}'} \frac{1}{v_F(\mathbf{k}')} \tilde{\Gamma}_{\mu\nu}^{even}(\mathbf{k}, \mathbf{k}') g_a(\mathbf{k}') = \lambda_a g_a(\mathbf{k}), \quad (8)$$

where the subscript a stands for different solutions. For a given eigenvalue λ_a , its eigenfunction $g_a(\mathbf{k})$ determines the symmetry of the gap, which could be s -wave or d -wave. An s -wave state is characterized by $g_a(\mathbf{k}) = g_a(\mathcal{R}\mathbf{k})$ and d -wave by $g_a(\mathbf{k}) = -g_a(\mathcal{R}\mathbf{k})$, where \mathcal{R} is the 90° -rotational operation on \mathbf{k} . Among the s -wave solutions, we pick up the largest one and set it to be λ_s and its eigenfunction to be g_s . Similarly, for the d -wave, they are denoted by λ_d and g_d . The eigenvalue equation Eq. (7) is not identical to the Bethe-Salpeter equation in which unity of eigenvalue stands for the formation of superconductivity. Instead, eigenvalues in Eq. (7) stand for the pairing strength. Therefore, the SC state is determined by largest one of λ_s and λ_d .

III. NUMERICAL RESULTS

A. Scattering Matrix

The scattering matrix shows some clues to the gap function. In order to gain more condensation energy, the gap should be larger in the region where the scattering matrix is maximal in magnitude. As the interaction is repulsive, the gap becomes anisotropic and sign-changing. Fig. 2 shows the "weighted" scattering matrix $[v_F(\mathbf{k})v_F(\mathbf{k}')]^{-1}\tilde{\Gamma}_{\mu\nu}^{even}(\mathbf{k},\mathbf{k}')$ for $U=1.0\text{eV}$ and $J_H=0.2U$. Here because the inverse Fermi velocity (IFV), $1/v_F(\mathbf{k})$, is related to the density of states (DOS), it is used as a weighting factor at each point. The scattering matrix contains intra and inter pocket scattering channels and different pockets are discriminated by the white dotted lines. The angles, $\theta_{\alpha 1}$, $\theta_{\alpha 2}$, $\theta_{\beta 1}$ and $\theta_{\beta 2}$ parametrizing momenta $\mathbf{k}(\mathbf{k}')$, increase from 0° to 360° as the coordinate increases from the bottom (left) to the top (right). Although we only show the result from one of the electron pocket β_1 (β_2), due to the nature of being even parity for $\tilde{\Gamma}_{\mu\nu}^{even}(\mathbf{k},\mathbf{k}')$, the result at the inversion point can be deduced.

In Fig. 2, the intra-electron-pocket (β_1 - β_1 or β_2 - β_2) scattering is much stronger than other channels and gives peaks at two momenta, which are at $\theta_{\beta 1} \approx 48^\circ$ and 225° as the antipodes (on the major axis) of the electron pockets. The strong intensity of the scattering matrix at these two momenta is expected because large IFV happens about the antipodes of the elliptic FS ($1/v_F(\mathbf{k})$ is shown in Fig. 5). One of the reasons why intra-electron-pocket scattering is strong is due to the much larger DOS on the electron pockets. This also explains why the inter-electron-hole-pocket scattering is stronger than the intra- and the inter-hole-pocket scattering. Furthermore, the intra-electron-pocket scattering comes from exchange of fluctuations at vectors $\mathbf{q} \approx \mathbf{0}$ and (π, π) , and the latter is driven by the substantial checkerboard antiferromagnetic fluctuations. The strength of DOS, however, can not explain why the inter-electron-pocket (β_1 - β_2) scattering is much small because the stripe antiferromagnetic fluctuations ($\mathbf{q}=(\pi, 0)$) are not weak at all. From the rotation symmetry argument⁴⁰, the orbital components on FS- β s are highly different (strictly speaking, belonging to different Fe atoms). The fluctuation exchange formula in Eq. (2) indicates that the inter-orbital fluctuations are heavily reduced. We have examined the case of neglecting the orbital-band matrix elements in Eq. (6) by setting $A_{a\mu}(\mathbf{k})=1/\sqrt{12}$ and find that the inter-electron-pocket scattering becomes comparable to the intra-electron-pocket one. Therefore, the small inter-electron-pocket scattering is due to the small magnitude of orbital-band matrix element.

B. Phase Diagram of Superconductivity

After a better understanding of the scattering matrix, we now show the results of eigenvalues from the eigenvalue problem in Eq. (8). Fig. 3 displays the largest eigenvalues of s -wave (λ_s) and d -wave (λ_d) as functions of U in three Hund's rule couplings, $J_H=0$, $0.2U$ and $0.4U$. λ_s is represented by solid blue lines while λ_d is represented by dashed red ones. As the interaction U is increased, quantum fluctuations enhances the SC pairing and then λ 's increase. Moreover, we observe that at different J_H , the dimensionless coupling constants for different symmetry grow in different speeds. As shown in the insets where the differences of two eigenvalues $\Delta\lambda \equiv \lambda_s - \lambda_d$ are plotted, the d -wave is always more stable against the s -wave ($\Delta\lambda < 0$) at $J_H=0$, while the preference is reverse ($\Delta\lambda > 0$) at $J_H=0.4U$. Between them at $J_H=0.2U$, the d -wave is favored for $U \lesssim 1.0\text{eV}$ but becomes unfavorable above that.

The above results indicate that the Hund's rule coupling is a parameter of controlling the SC symmetry as well as the AFM order⁴⁰. This is further supported by Fig. 4, in which $\Delta\lambda$ versus J_H at different U is plotted. Except for the small phase space with $U=1.0\text{eV}$ and $J_H < 0.4U$, $\Delta\lambda$ increases monotonously with J_H , indicating that the Hund's rule coupling favors the s -wave. However, $\Delta\lambda$ is not a monotonic function of U . There exists a critical J_H , $J_{H,c} \approx 0.2U$, separating two states; below it, $\Delta\lambda$ decreases as U increases, but above it, $\Delta\lambda$ increases with U .

C. Gap Functions

With the phase diagram of superconductivity, one still needs to know the gap function explicitly to understand its physics, especially in this new type of system with space group different from other iron-based superconductors. We shall first examine the case of s -wave solution in Fig. 5 and then the d -wave one in Fig. 6.

1. s -wave

Following Ref.[6], we shall speak of s -wave by $g_a(\mathcal{R}\mathbf{k}) = g_a(\mathbf{k})$ with \mathcal{R} being the 90° -rotational operation on \mathbf{k} . Fig. 5 shows the s -wave gap function $g_s(\mathbf{k})$ along FS sheets α_1 , α_2 , and β_1 for $U=1.0\text{eV}$ and $J_H=0.2U$. $g_s(\mathbf{k})$ on FS- β_2 not shown is the same as on FS- β_1 when $\theta_{\beta 2} = \theta_{\beta 1}$. Blue squares are the eigenvalue-problem solution, while the solid red lines are the fit guided by eye. One of the features is that such defined s -wave gap have multi-nodes on FS- α_1 , β_1 and β_2 . Moreover, because there is no reflection symmetry, there is an extra degree of freedom in defining the zero value of angles. As a result, the fitting curves for s -wave symmetry,

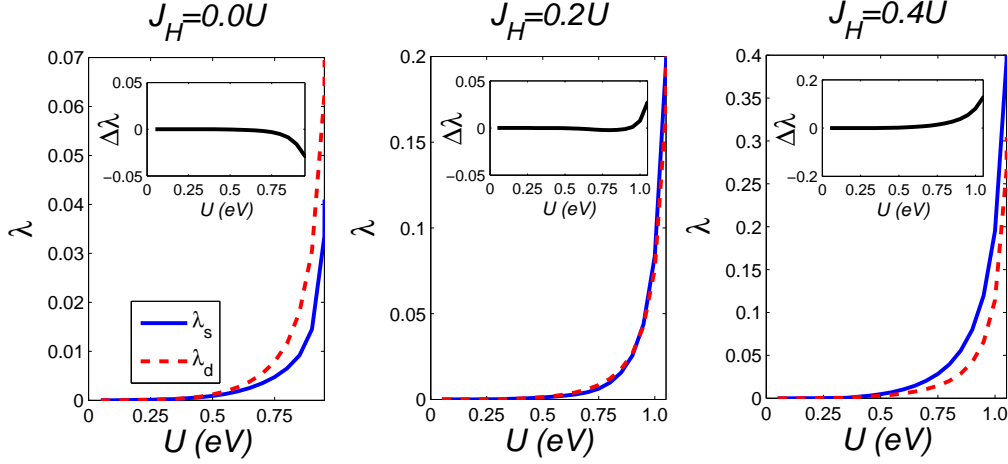


FIG. 3: (Color online) Eigenvalues or dimensionless coupling constants λ_s (s -wave) and λ_d (d -wave) as functions of U for $J_H=0, 0.2U$, and $0.4U$ from the left panel to the right one. Solid blue lines are for λ_s and dashed red ones are for λ_d . Insets are the difference of eigenvalues, $\Delta\lambda = \lambda_s - \lambda_d$, to exhibit the favorable state. The eigenvalues for $J_H=0$ are smaller, but they grow up fast and solutions become unstable at about $U=1.0\text{eV}$

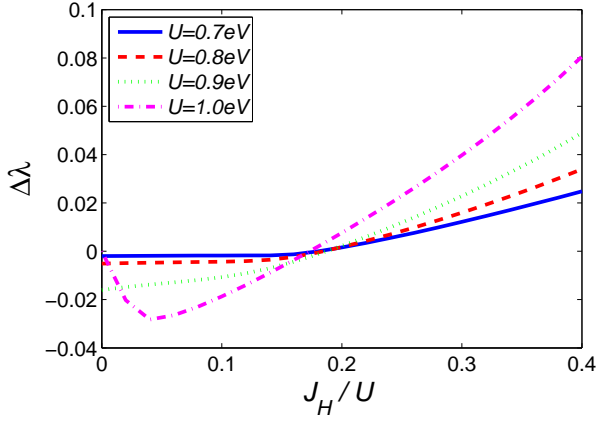


FIG. 4: (Color online) The eigenvalue differences between the s -wave and the d -wave, $\Delta\lambda$, as functions J_H/U in four cases of U : $U=0.7\text{eV}$ (solid blue), $U=0.8\text{eV}$ (red dashed), $U=0.9\text{eV}$ (dotted green), and $U=1.0\text{eV}$ (dash-dotted pink). A critical J_H ($\approx 0.2U$) is observed as the transition point between s -wave and d -wave.

chosen from lowest harmonic functions, are found to be

$$\begin{aligned} g_s(\theta_{\alpha 1}) &= 0.031 \cos[4(\theta_{\alpha 1} - 1^\circ)] + 0.0153, \\ g_s(\theta_{\alpha 2}) &= 0.028 \cos[4(\theta_{\alpha 2} + 5^\circ)] \\ &\quad + 0.008 \cos[8(\theta_{\alpha 2} - 22^\circ)] - 0.136, \\ g_s(\theta_{\beta 1}) &= -0.13 [\cos(k'_x) + \cos(k'_y)] \\ &\quad + 0.4 \cos(k'_x) \cos(k'_y) + 0.37, \end{aligned} \quad (9)$$

where $k'_x = k_x \cos(20^\circ) - k_y \sin(20^\circ)$, $k'_y = k_x \sin(20^\circ) + k_y \cos(20^\circ)$. Here $\cos 4\theta$, $\cos 8\theta$, $\cos(k_x) + \cos(k_y)$, and $\cos(k_x) \cos(k_y)$ are the common s -wave bases. (Because FS- β_1 is not located on symmetric point, a different type

of bases is adopted.) However, due to the broken of reflection symmetry, zeros of angles get shifted by 1° , -5° , 22° and 20° . These angles are the allowed degrees of freedom in the C_{4h} symmetry and their precise values are to minimize the total energy of the system.

Similar to the s^\pm -wave proposed in iron-pnictide superconductor⁴⁶, where the SC order parameter on hole pockets and on electron pockets have opposite signs to make superconductivity stable, here we have the similar mechanism. In Fig. 5, we see that the mean value of the gap on FS- α_2 has an opposite sign to those on FS- α_1 and FS- β 's, which suggests these inter-pocket scatterings gain energy. Due to their larger scattering strength, the $\alpha_2 - \beta$'s scattering processes gain most energy. The $\alpha_1 - \beta$'s scattering processes are not favorable due to large cancellation by the oscillating behavior between positive and negative of gap on FS- α_1 . For the intra-pocket scattering processes, because the Fermi surfaces are small and if the fluctuations are smooth over the wave vector \mathbf{q} , it would be not able to change the interaction from repulsive to attractive. However, the repulsive strength can be reduced by making the gap oscillatory and even with the sign being changed. The reason why the gap functions take the particular forms of Eq.(9) can be answered if we look at the IFV by the dashed green lines in Fig. 5. Clearly, the oscillating gap function results from the oscillating IFV. On FS- β_1 , the IFV is peaked at $\theta_{\beta 1} \approx 225^\circ$ where the gap is a peak too. The fact that the other point at $\theta_{\beta 1} \approx 48^\circ$ with high IFV does not lead to a large gap is because the repulsion can be lowered in the intra- and inter-electron-pocket scattering processes. The fact that the gap on FS- α_2 being in-phase with the IFV and having no sign-reversal leads to more energy gained from the $\alpha_2 - \beta$'s scattering processes but it leads to energy loss from the intra-pocket scattering. On the other hand, the gap function on FS- α_1 is about $\frac{\pi}{2}$ -out-of-phase rela-

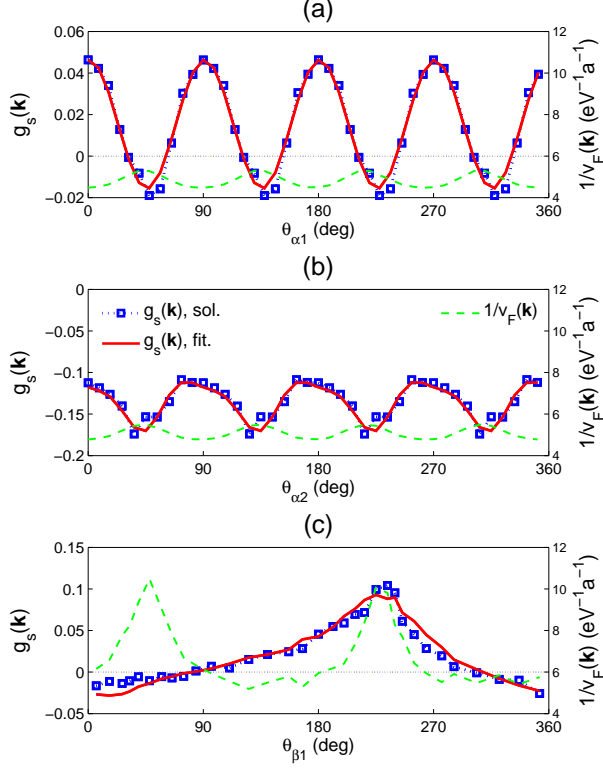


FIG. 5: (Color online) s -wave eigenfunction $g_s(\mathbf{k})$ for $U=1.0\text{eV}$ and $J_H=0.2U$. Panel (a) is along FS- α_1 , (b) along FS- α_2 , and (c) along FS- β_1 . Blue squares are the eigenvalue-problem solution and the solid red lines are fitting curves (function forms are seen in the main context). Due to the s -wave character, the gap function on FS- β_1 and FS- β_2 is related by $g_s(\theta_{\beta 2}) = g_s(\theta_{\beta 1})$ when $\theta_{\beta 2} = \theta_{\beta 1}$. The factor, $1/v_F(\mathbf{k})$, which is proportional to DOS, is also shown by the dashed green lines. a is the lattice length, which from transmission electron microscopy⁴⁵ is about 6.15\AA .

tive to the IFV, which would be a compromise between the intra- and inter-pocket scattering processes. In below, we list the numerical result of the coupling matrix $\hat{\lambda}_s/\lambda_s$, which is consistent with the above demonstration:

$$\frac{\hat{\lambda}_s}{\lambda_s} = \begin{bmatrix} -0.0275 & 0.2628 & -0.1039 & -0.1039 \\ & -2.8292 & 1.6033 & 1.6033 \\ & & -1.1398 & -0.1947 \\ & & & -1.1398 \end{bmatrix},$$

where due to that $\hat{\lambda}_s$ is a symmetric matrix, the lower-triangular matrix elements are omitted for brevity, and $\lambda_s = \sum_{\mu,\nu} (\hat{\lambda}_s)_{\mu\nu} = 0.0837$.

2. d -wave

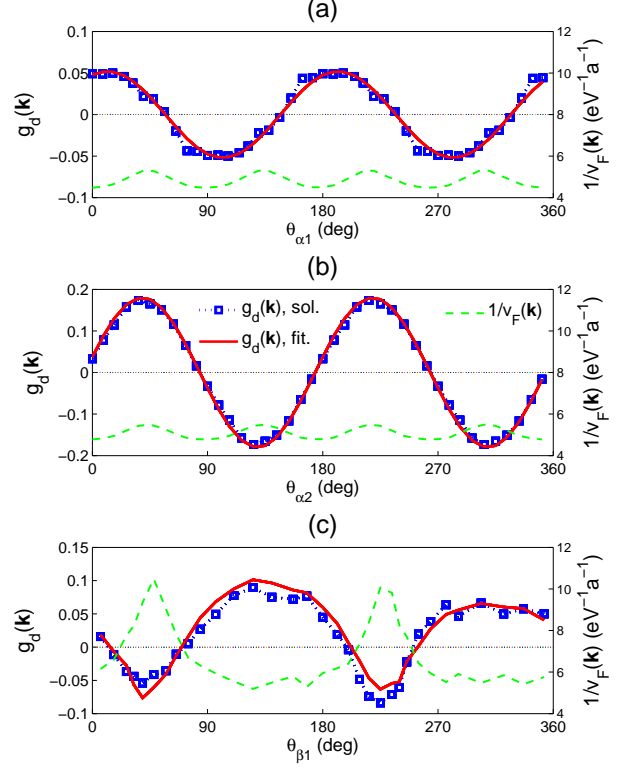


FIG. 6: (Color online) d -wave eigenfunction $g_d(\mathbf{k})$ for $U=0.9\text{eV}$ and $J_H=0.0$. Due to the d -wave character, $g_d(\theta_{\beta 2}) = -g_d(\theta_{\beta 1})$ when $\theta_{\beta 2} = \theta_{\beta 1}$. The plot representation is the same as in Fig. 5 while the fitting curves are different and are discussed in the text.

Similar to the s -wave, the d -wave that we shall speak of obeys $g_d(\mathcal{R}\mathbf{k}) = -g_d(\mathbf{k})$ with \mathcal{R} being the 90° -rotational operation on \mathbf{k} . In Fig. 6, we show the d -wave gap function $g_d(\mathbf{k})$ for $U=0.9\text{eV}$ and $J_H=0.0$. $g_d(\mathbf{k})$'s on FS- β_1 and FS- β_2 are equal in magnitude but has opposite signs, *i.e.*, $g_d(\theta_{\beta 2}) = -g_d(\theta_{\beta 1})$ when $\theta_{\beta 2} = \theta_{\beta 1}$. It is seen that the gap functions of d -wave always have nodes on any Fermi surface. The fitted functions in Fig. 6 (solid red) are given by

$$\begin{aligned} g_d(\theta_{\alpha 1}) &= 0.052 \cos[2(\theta_{\alpha 1} - 12^\circ)], \\ g_d(\theta_{\alpha 2}) &= 0.18 \cos[2(\theta_{\alpha 2} - 39^\circ)], \\ g_d(\theta_{\beta 1}) &= 0.12 [\cos(k'_x) - \cos(k'_y)] \\ &\quad - 0.34 \sin(k''_x) \sin(k''_y), \end{aligned} \quad (10)$$

where $k'_x = k_x \cos(2^\circ) + k_y \sin(2^\circ)$, $k'_y = -k_x \sin(2^\circ) + k_y \cos(2^\circ)$, $k''_x = k_x \cos(1^\circ) - k_y \sin(1^\circ)$, and $k''_y = k_x \sin(1^\circ) + k_y \cos(1^\circ)$. Note that instead of being $\cos 4\theta$ (which is for the s -wave), d -wave is represented by $\cos 2\theta$. Similar to the s -wave case, zeros of angles also get shifted although nodes appear on every FS sheet, they are not at the diagonal directions.

The major difference between d -wave and s -wave lies in the sign-changing property of d -wave, which reduces repulsion in intra-pocket and inter-electron-pocket scatterings. Similar to cuprate superconductors, this mechanism turns the pair coupling into attraction. As a result, both antipodes on FS- β_1 ($\theta_{\beta 1} \approx 48^\circ$ and 225°) have large gaps in Fig. 6, in comparison to a single hump in Fig. 5. The coupling constant matrix $(\hat{\lambda}_d)_{\mu\nu}$ summarizes the above effects

$$\frac{\hat{\lambda}_d}{\lambda_d} = \begin{bmatrix} 0.0033 & 0.0361 & 0.0066 & 0.0066 \\ & -0.0393 & 0.2623 & 0.2623 \\ & & -0.0459 & -0.0066 \\ & & & -0.0459 \end{bmatrix},$$

where $\lambda_d = \sum_{\mu,\nu} (\hat{\lambda}_d)_{\mu\nu} = 0.0305$. Note that not only the repulsion between intra-pocket electrons is reduced, because of the presence of nodes, the attraction between inter-pocket electrons is also reduced. Although the d -wave state might not gain much energy from inter-pocket scattering processes relative to the s -wave state, it saves more energy from the reduction of intra-pocket repulsion.

IV. SUMMARY

In summary, proximity of antiferromagnetism and superconductivity in $\text{A}_y\text{Fe}_{1.6}\text{Se}_2$ implies that the SC state could be derived from spin fluctuations. Under this assumption and assuming that superconductivity exists in the $\sqrt{5} \times \sqrt{5}$ iron-vacancy ordering state, we study the SC states from the effective pairing interaction in the FLEX approximation based on our previous 12-orbital

tight-binding model⁴⁰. Similar to that of iron-pnictide superconductors, for the spin-singlet superconductivity, s -wave and d -wave states are found to be close in energy. In particular, a quantum critical point is found at $J_H \approx 0.2U$, below which the d -wave prevails, while above which the s -wave wins over. Furthermore, unlike the iron-pnictide superconductors, the iron-vacancy order lowers the symmetry to the group C_{4h} so that the gap functions do not need to be reflection symmetric. As a result, it implies that there are degrees of freedom in defining zeros of angles for the pairing momenta. These extra degrees of freedom for the gap functions can further increase the gain of the condensation energy.

Finally, while our work focus on the superconductivity, the finding of quantum critical point controlled by J_H in superconductivity is not an accident. In the magnetism, we have shown⁴⁰ that J_H controls the magnetic phase transition from stripe to checkerboard AFM. In addition, it is also shown that the crossover between coherence and incoherence is also determined by J_H ⁴³. Together with the observed pressure-driven magnetic phase transition^{20,21}, which accompanies the metal-to-semiconductor transition, we conclude that the Hund's rule coupling performs the dominant role in determining localization, magnetism, and superconductivity of iron-based superconductors.

Acknowledgments

We thank Dr. Ming-Chang Chung for useful discussions. This work was supported by the National Science Council of Taiwan.

-
- ¹ G. R. Stewart, Rev. Mod. Phys. **83**, 1589 (2011).
 - ² H. Oh, J. Moon, D. Shin, C.-Y. Moon, and H. J. Choi, Progress in Superconductivity **13**, 65-84 (2011).
 - ³ K. Kuroki, S. Onari, R. Arita, H. Usui, Y. Tanaka, H. Kontani, and H. Aoki, Phys. Rev. Lett. **101**, 087004 (2008).
 - ⁴ I.I. Mazin and J. Schmalian, Physica C **469**, 614 (2009).
 - ⁵ H. Zhai, F. Wang, and D.-H. Lee, Phys. Rev. B **80**, 064517 (2009).
 - ⁶ S. Graser, T. A. Maier, P. J. Hirschfeld, and D. J. Scalapino, New J. Phys. **11**, 025016 (2009).
 - ⁷ J. Guo, S. Jin, G. Wang, S. Wang, K. Zhu, T. Zhou, M. He, and X. Chen, Phys. Rev. B **82**, 180520(R) (2010).
 - ⁸ W. Bao, Q. Huang, G. F. Chen, M. A. Green, D. M. Wang, J. B. He, X. Q. Wang, and Y. Qiu, Chin. Phys. Lett. **28**, 086104 (2011).
 - ⁹ J. Bacsá, A. Y. Ganin, Y. Takabayashi, K. E. Christensen, K. Prassides, M. J. Rosseinsky, and J. B. Claridge, Chem. Sci. **2**, 1054 (2011).
 - ¹⁰ X.-W. Yan, M. Gao, Z.-Y. Lu, and T. Xiang, Phys. Rev. B **83**, 233205 (2011).
 - ¹¹ M. H. Fang, H. D. Wang, C. H. Dong, Z. J. Li, C. M. Feng, J. Chen, and H. Q. Yuan, Europhys. Lett. **94**, 27009 (2011).
 - ¹² D. M. Wang, J. B. He, T.-L. Xia, and G. F. Chen, Phys. Rev. B **83**, 132502 (2011).
 - ¹³ Z. Wang, Y. J. Song, H. L. Shi, Z. W. Wang, Z. Chen, H. F. Tian, G. F. Chen, J. G. Guo, H. X. Yang, and J. Q. Li, Phys. Rev. B **83**, 140505(R) (2011).
 - ¹⁴ B. Shen, B. Zeng, G. F. Chen, J. B. He, D. M. Wang, H. Yang, and H. H. Wen, Europhys. Lett. **96**, 37010 (2011).
 - ¹⁵ D. H. Ryan, W. N. Rowan-Weetaluktuk, J. M. Cadogan, R. Hu, W. E. Straszheim, S. L. Bud'ko, and P. C. Canfield, Phys. Rev. B **83**, 104526 (2011).
 - ¹⁶ F. Chen, M. Xu, Q. Q. Ge, Y. Zhang, Z. R. Ye, L. X. Yang, Juan Jiang, B. P. Xie, R. C. Che, M. F. Zhang, A. F. Wang, X. H. Chen, D. W. Shen, J. P. Hu, and D. L. Feng, Phys. Rev. X **1**, 021020 (2011).
 - ¹⁷ A. Ricci, N. Poccia, G. Campi, B. Joseph, G. Arrighetti, L. Barba, M. Reynolds, M. Burghammer, H. Takeya, Y. Mizuguchi, Y. Takano, M. Colapietro, N. L. Saini, and A. Bianconi, Phys. Rev. B **84**, 060511(R) (2011).
 - ¹⁸ R. H. Yuan, T. Dong, Y. J. Song, G. F. Chen, J. P. Hu, J. Q. Li, and N. L. Wang, e-print arXiv:1102.1381 (unpublished).
 - ¹⁹ W. Li, H. Ding, P. Deng, K. Chang, C. Song, K. He, L. Wang, X. Ma, J. P. Hu, X. Chen, and Q. K. Xue, Nature

- Phys. (2011) doi:10.1038/nphys2155.
- ²⁰ L. Chen, X. W. Yan, Z. Y. Lu, and T. Xiang, e-print arXiv:1109.3049 (unpublished).
 - ²¹ J. Guo, X. Chen, C. Zhang, J. Guo, X. Chen, Q. Wu, D. Gu, P. Gao, X. Dai, L. Yang, H. K. Mao, L. Sun, and Z. Zhao, arXiv:1101.0092 (unpublished).
 - ²² Y. Liu, Z. C. Li, W. P. Liu, G. Friemel, D. S. Inosov, R. E. Dinnebier, Z. J. Li, and C. T. Lin, e-print arXiv:1201.0902 (unpublished).
 - ²³ W. Yu, L. Ma, J. B. He, D. M. Wang, T.-L. Xia, G. F. Chen, and W. Bao, Phys. Rev. Lett. **106**, 197001 (2011).
 - ²⁴ D. A. Torchetti, M. Fu, D. C. Christensen, K. J. Nelson, T. Imai, H. C. Lei, and C. Petrovic, Phys. Rev. B **83**, 104508 (2011).
 - ²⁵ L. Ma, G. F. Ji, J. Zhang, J. B. He, D. M. Wang, G. F. Chen, W. Bao, and W. Yu, Phys. Rev. B **83**, 174510 (2011).
 - ²⁶ The relevant spin fluctuation in this system is the checkerboard AFM fluctuation at $\mathbf{q}=(\pi,\pi)$, which is not revealed in the Knight shift K as being related to the spin susceptibility at $\mathbf{q}=0$. For $1/T_1 T$ on Se or on the mono-valence element A which locates at the center of the iron square, the form factor⁶ and iron deficiencies would suppress the effect of the checkerboard AFM fluctuation.
 - ²⁷ A. M. Zhang, J. H. Xiao, Y. S. Li, J. B. He, D. M. Wang, G. F. Chen, B. Normand, Q. M. Zhang, and T. Xiang, e-print arXiv:1106.2706 (unpublished).
 - ²⁸ T. A. Maier, S. Graser, P. J. Hirschfeld, and D. J. Scalapino, Phys. Rev. B **83**, 100515(R) (2011).
 - ²⁹ F. Wang, F. Yang, M. Gao, Z. Y. Lu, T. Xiang, and D. H. Lee, Europhys. Lett. **93**, 57003 (2011).
 - ³⁰ Y. Zhou, D. H. Xu, F. C. Zhang, and W. Q. Chen, Europhys. Lett. **95**, 17003 (2011).
 - ³¹ T. Das and A. V. Balatsky, Phys. Rev. B **84**, 014521 (2011).
 - ³² I. I. Mazin, Phys. Rev. B **84**, 024529 (2011).
 - ³³ I. R. Shein and A. L. Ivanovskii, e-print arXiv:1012.5164 (unpublished).
 - ³⁴ C. Cao and J. Dai, Chin. Phys. Lett. **28**, 057402 (2011).
 - ³⁵ C. Cao and J. Dai, Phys. Rev. Lett. **107**, 056401 (2011).
 - ³⁶ Y. Zhang, L. X. Yang, M. Xu, Z. R. Ye, F. Chen, C. He, H. C. Xu, J. Jiang, B. P. Xie, J. J. Ying, X. F. Wang, X. H. Chen, J. P. Hu, M. Matsunami, S. Kimura, and D. L. Feng, Nat. Mater. **10**, 273 (2011).
 - ³⁷ D. Mou, S. Liu, X. Jia, J. He, Y. Peng, L. Zhao, L. Yu, G. Liu, S. He, X. Dong, J. Zhang, H. Wang, C. Dong, M. Fang, X. Wang, Q. Peng, Z. Wang, S. Zhang, F. Yang, Z. Xu, C. Chen, and X. J. Zhou, Phys. Rev. Lett. **106**, 107001 (2011).
 - ³⁸ T. Qian, X.-P. Wang, W.-C. Jin, P. Zhang, P. Richard, G. Xu, X. Dai, Z. Fang, J.-G. Guo, X.-L. Chen, and H. Ding, Phys. Rev. Lett. **106**, 187001 (2011).
 - ³⁹ L. Zhao, D. Mou, S. Liu, X. Jia, J. He, Y. Peng, L. Yu, X. Liu, G. Liu, S. He, X. Dong, J. Zhang, J. B. He, D. M. Wang, G. F. Chen, J. G. Guo, X. L. Chen, X. Wang, Q. Peng, Z. Wang, S. Zhang, F. Yang, Z. Xu, C. Chen, and X. J. Zhou, Phys. Rev. B **83**, 140508(R) (2011).
 - ⁴⁰ S. M. Huang and C. Y. Mou, Phys. Rev. B **84**, 184521 (2011).
 - ⁴¹ N. E. Bickers, D. J. Scalapino, and S. R. White, Phys. Rev. Lett. **62**, 961 (1989).
 - ⁴² T. Takimoto, T. Hotta, and K. Ueda, Phys. Rev. B **69**, 104504 (2004).
 - ⁴³ K. Haule and G. Kotliar, New J. Phys. **11**, 025021 (2009).
 - ⁴⁴ D. Scalapino, E. Loh, and J. Hirsch, Phys. Rev. B **34**, 8190 (1986).
 - ⁴⁵ Z. Wang, Y. J. Song, H. L. Shi, Z. W. Wang, Z. Chen, H. F. Tian, G. F. Chen, J. G. Guo, H. X. Yang, and J. Q. Li, Phys. Rev. B **83**, 140505(R) (2011).
 - ⁴⁶ I. I. Mazin, D. J. Singh, M. D. Johannes, and M. H. Du, Phys. Rev. Lett. **101**, 057003 (2008).